Urban Climate 17 (2016) 196–215

Contents lists available at ScienceDirect

Urban Climate

journal homepage: http://www.elsevier.com/locate/uclim

Linking urban climate classification with an urban energy and water budget model: Multi-site and multi-seasonal evaluation

P.J. Alexander [a,*], B. Bechtel [b], W.T.L. Chow [c], R. Fealy [d], G. Mills [e]

[a] Irish Climate Analysis & Research Units, Maynooth University, Co. Kildare, Ireland
[b] Institute of Geography, University of Hamburg, Hamburg, Germany
[c] Department of Geography, National University of Singapore, Singapore
[d] Department of Geography, Maynooth University, Co. Kildare, Ireland
[e] School of Geography, University College Dublin, Dublin, Ireland

ARTICLE INFO

Article history:
Received 4 February 2016
Received in revised form 8 August 2016
Accepted 10 August 2016

Keywords:
UEB
SUEWS
LCZ
Urban model evaluation
Flux measurements

ABSTRACT

There are a number of models available for examining the interaction between cities and the atmosphere over a range of scales, from small scales - such as individual facades, buildings, neighbourhoods - to the effect of the entire conurbation itself. Many of these models require detailed morphological characteristics and material properties along with relevant meteorological data to be initialised. However, these data are difficult to obtain given the heterogeneity of built forms, particularly in newly emerging cities. Yet, the need for models which can be applied to urban areas (for instance to address planning problems) is increasingly urgent as the global population becomes more urban. In this paper, a modeling approach which derives the required land cover parameters for a mid-complex urban energy budget and water budget model (SUEWS) in a consistent manner is evaluated in four cities (Dublin, Hamburg, Melbourne and Phoenix). The required parameters for the SUEWS model are derived using local climate zones (LCZs) for land cover, and meteorological observations from off-site synoptic stations. More detailed land cover and meteorological data are then added to the model in stages to examine the impact on model performance with respect to observations of turbulent fluxes of sensible (Q_H) and latent (Q_E) heat. Replacing LCZ land cover with detailed fractional coverages was shown to marginally improve model performance, however the performance of model coupled with 'coarse' LCZ data was within

* Corresponding author.
E-mail address: paul.alexander@nuim.ie (P.J. Alexander)

http://dx.doi.org/10.1016/j.uclim.2016.08.003

the same range of error (20–40 W m^{-2} for Q_E and 40–60 W m^{-2} for Q_H) as high resolution data.

1. Introduction

There has been considerable progress in the representation of urban-scale processes within atmospheric models. A variety of urban-scale models now exist which are capable of simulating the urban heat island either empirically or using physical models (Taha et al., 1988; Myrup, 1969; Atkinson, 2003; Bottyán and Unger, 2003; Kusaka and Kimura, 2004; Hoffmann et al., 2012), urban air quality (Shir and Shieh, 1974; Huang et al., 2000; Karppinen et al., 2000), human thermal comfort in the outdoor urban environment (de Dear and Brager, 1998; Ali-Toudert and Mayer, 2006), energy demand and anthropogenic emissions of heat (Block et al., 2004; Fan and Sailor, 2005; Allen et al., 2011). There are a wide number of surface schemes for modeling fluxes of mass, momentum and energy in urban areas (i.e. the urban energy balance - UEB), which vary in complexity in terms of their parameterisation and hence, their input requirements. More complex UEB schemes have been shown to be very useful in examining, for instance, the detailed hygrothermal impact of different urban forms and functions on the micro-scale climate (Barlow et al., 2004; Harman et al., 2004; Dupont et al., 2004). Such models are invaluable for understanding the processes in operation within urban environments. Moreover, there are some examples of where UEB models have been coupled with meso-scale models (Harman and Belcher, 2006; Bueno et al., 2013; Stewart et al., 2014; Onomura et al., 2015; De Ridder et al., 2015) which would effectively allow for micro-scale meteorological forecasts.

These complex UEB models however are incapable of being run in many data poor settings, or at least routinely, for cities in the economically developing world where the application of such models to planning problems and adaptation to extreme weather conditions would have the largest potential benefit. There is now a clear need to overcome this knowledge gap so as to allow greater integration of urban climate knowledge with the planning and policy communities (Mills et al., 2010; Ching, 2013; Hebbert and Mackillop, 2013; Heaphy, 2015). For instance, a comparison of 33 models by Grimmond et al. (2010) highlighted the large number (145) of input parameters required by the group of models considered. Providing such parameters for a single neighbourhood is challenging, and this is before we consider the parameters required for an entire urban area. In order to carry out simulations across an entire urban domain, generalisations will be needed in the interim.

Obtaining the necessary input parameters in data poor settings is only part of the problem, greater rigour in evaluating models in differing background climates and in different cities is also urgently needed. As stated by Oke (2006), without extensive model evaluation exercises the utility of UEB models for planning problems remains dubious. The international urban climate model comparison (Grimmond et al., 2010; Grimmond et al., 2011) went a large way towards discovering the general ability of UEB models in simulating the urban effect on turbulent fluxes and prioritising the most important input parameters. Research on specific model performance in different settings is also beginning to emerge (Loridan and Grimmond, 2012). Despite this there is still a noted lack of integration of urban climate knowledge in the planning process. Very few examples exist of UEB models being applied to real planning problems in collaboration with city planners (Eliasson, 2000). In order to bridge this knowledge gap, more specific evaluation of individual UEB models needs to be undertaken, with clearer links to planning applications, as proposed by Masson et al. (2014). It is unlikely that there will emerge a one-model-fits-all scheme that will apply to all situations, however a starting point may be to seek a balance between realistically representing urban processes, ensuring good model accuracy and requiring readily obtained input parameters that are derived in a consistent manner so as to allow inter-city comparisons.

While concerted effort has been placed on model development (Hidalgo et al., 2008) to better represent urban climate processes and move towards operational use in forecasting models, there is a clear need for more general models which are also capable of studying the impacts of urbanisation on the environment with fewer input requirements. One example is the local scale urban meteorological parameterisation scheme (LUMPS – Grimmond and Oke, 2002) which has been shown to accurately simulate the UEB in multiple cities requiring only simple input parameters. The simple treatment of vegetation and water availability i.e. urban water balance (UWB) within LUMPS limits its application to real planning challenges. Hence a mid-complex

scheme, the surface urban energy and water balance scheme (SUEWS – Järvi et al., 2011) was subsequently developed which has a high potential to fill this intermediate space between complex parameterisation, accuracy and ease of implementation.

SUEWS requires more input parameters than LUMPS, however it is still relatively straightforward to carry out simulations and due to its inclusion of the UWB can be applied for planning problems. The model has already been evaluated in Helsinki, Los Angeles (Järvi et al., 2011; Järvi et al., 2014) and Dublin (Alexander et al., 2015) where the necessary inputs to force the model and evaluate its performance were available.

Here we evaluate SUEWS further in three additional background climates and urban configurations. However, our primary aim is to consider the impact of data quality and evaluate model accuracy in a systematic way across multiple sites. In order to derive a means to apply SUEWS in data poor situations we employ a modeling approach which links the local climate zone (LCZ) classification (Stewart and Oke, 2012) with SUEWS. LCZ are linked with SUEWS to derive the necessary land cover parameters easily and in a consistent manner across an entire urban domain. Here, we extend the proof of concept established in a previous paper (Alexander et al., 2015) to include additional background climates and multiple urban environments in order validate the LCZ-SUEWS approach and answer the following questions:

1) Can off-site meteorological data be used to force SUEWS and what is the impact on performance?
2) Is the impact of "low quality" (i.e. LCZ) land cover data on SUEWS performance comparable across different cities?

The answer to these questions will have a direct impact on applying the model in data-poor settings such as rapidly expanding urban areas. Prior to outlining the methods employed in this paper, the use of LCZ with the SUEWS model is discussed.

2. LCZ-SUEWS approach

The traditional approach for modeling urban areas involves a number of procedures. Firstly, the urban area is parameterised in terms of fraction coverage (λ) of buildings, roads and pathways, vegetation, soils and water. Building form (morphology) and vegetation are then derived based either from LiDAR, aerial imagery or field work. From these other parameters are derived for example the sky view factor (ψ) and height/width (H/W) ratio. The function (as well building materials) is derived using local expert knowledge. Finally, the derivation of meteorological forcing data, either from observations made on site or through an atmospheric model such as a regional climate model. A number of different methods and data can be employed in each of these stages, a standard does not exist for any scale, and thus inter-site comparisons remain largely elusive. Moreover, in some data starved regions the availability of high-quality data (i.e. multispatial, multitemporal) required by some methods is sparse or simply non-existent.

The basic premise of the linked LCZ-SUEWS approach addresses this disparity. Rather than view the urban area as a collection of individual surfaces (walls, rooftops, roads, materials) the approach employs as its starting point the notion that the urban area is a collection of discrete homogenous neighbourhoods of similar characteristics, seeks to identify these neighbourhoods and standardise the approach for deriving parameters for these neighbourhoods required by models.

The thermal differentiation of urban areas using LCZ as a basis has already been demonstrated both empirically and through modeling (Fenner et al., 2014; Stewart et al., 2014; Leconte et al., 2015; Colunga et al., 2015). Moreover, the ability to identify LCZ across entire urban areas i.e. to map LCZ has also been demonstrated (Bechtel et al., 2015). Therefore, LCZ are ideally placed for standardising the collection of model parameters and for applying the outputs of UEB models across a much larger domain, thus reducing computational expense. There are a number of advantages of the approach:

1. The LCZ scheme itself is defined based on fractional coverages of different land cover types and urban parameters (building height/roughness, ψ and H/W) thus enables a first estimate of these parameters for models;
2. The classification of a city into LCZ enables subsequent strategic sampling of the urban area to derive detailed parameter values and characteristics such as building materials, population density and land use;
3. LCZ were designed to better describe the site characteristics of urban temperature sensors, hence can aid in the placement of instruments, the interpretation and evaluation of model simulations based on these observations;

4. The scheme was designed to be universally understood and since they employ standard building forms are likely to coincide (either in part or entirely) with other land use land cover classifications that have already been established (Alexander and Mills, 2014; Leconte et al., 2015).

Fig. 1 illustrates the approach in terms of linking LCZ to a UCM across multiple urban scales, highlighting points 1–4 from above. Methods are currently being tested to create LCZ maps for most cities using readily obtained open source data (Bechtel et al., 2015). Therefore, we are assuming for the approach either (i) a LCZ map of the urban area is available or (ii) another LULC map which can be translated into LCZ is available.

It should be noted there are only a few examples of where LCZ have been linked to microscale (≤100 m) models (see Middel et al. (2014) for example) essentially where subsets of a neighbourhood are examined using the LCZ framework. There are currently no examples in literature of linking LCZ to building scale (≤10 m) models. This may be possible in some instances where particular forms and functions can be inferred from individual LCZ classes (for instance, it would be unlikely LCZ 10 would ever describe a residential area and more likely to be required to conform to particular design/material regulations). While examining building scale through the LCZ may seem impractical, it potentially allows for later upscaling to micro, local and meso scale therefore may be useful. However, for this work the approach employs the local scale (500–1000 m) to derive model parameters and apply model outputs.

3. Experimental outline

We test the effect of using LCZ data which is derived in a consistent way on SUEWS performance by carrying out simulations of the UEB at four locations and compare the results against observations of turbulent fluxes of sensible (Q_H) and latent heat (Q_E). The SUEWS model (v.2014b) is outlined in detail in (Järvi et al., 2011) and (Järvi et al., 2014). In brief, the model calculates hourly radiative fluxes ($Q^* = K^* + L^*$) using the net all-wave radiation parameterisation (NARP - Offerle et al., 2003) latent heat, Q_E, using a modified Penman-Monteith equation (Grimmond and Oke, 1991) heat storage, ΔQ_S, using the Objective Hysteresis Model (OHM - Grimmond and Oke, 1999) and anthropogenic heat, Q_F, using the Sailor and Vasireddy approach (Sailor and Vasireddy, 2006). Finally, Q_H is calculated as the residual from the calculated fluxes i.e. $Q_H = Q^* - [Q_E + \Delta Q_S + Q_F]$.

3.1. Experimental setup

In order to evaluate the LCZ-SUEWS approach, we designed a systematic experiment to test the impact of improving data quality on model performance. Our evaluation is carried out in four cities. The locations and data descriptions are outlined in Section 3.2 below, here we provide an outline of the experimental procedure – see Table 1 for overview.

We adopted a similar approach to the inter-model comparison project (Grimmond et al., 2011) whereby SUEWS was initially run using baseline land cover parameters and off-site meteorology ("low" quality data sampled using LCZ maps). Subsequently more detailed land cover fractions and meteorological data were added in stages. Each step was intended to reveal the importance of information quality on the model output. Due to the uncertainty/assumptions required in relation to Q_F for several of the sites we opted to exclude this flux from the model runs – though estimates are provided for some of the sites which indicate the magnitude is low (≤30 W m^{-2}).

Data from urban flux observations sites and proximate WMO standard synoptic stations were obtained by contacting data holders at each of the four sites. Once these data were released and collated for a period of approximately one year for each site, we generated a LCZ classification following the method outlined in Bechtel et al. (2015) for each city where data were available. Land cover parameters were then derived by sampling LCZs (excluding the area surrounding the flux sites) and manually computing fractional coverages, this was done in Google Earth Pro similar to the method proposed by See et al. (2015). For high-resolution land cover we used the reported meta-data values for the flux sites. Where this was unavailable, we derived detailed fractional coverages, building heights and vegetation type(s) surrounding each of the sites out to radius of 500 m from the flux platforms.

The model was span up prior to each of the experiments using the following approach: for each of the sites, we saturated the surrounding landscape i.e. soil moisture content (SMC) was set to maximum, and the model

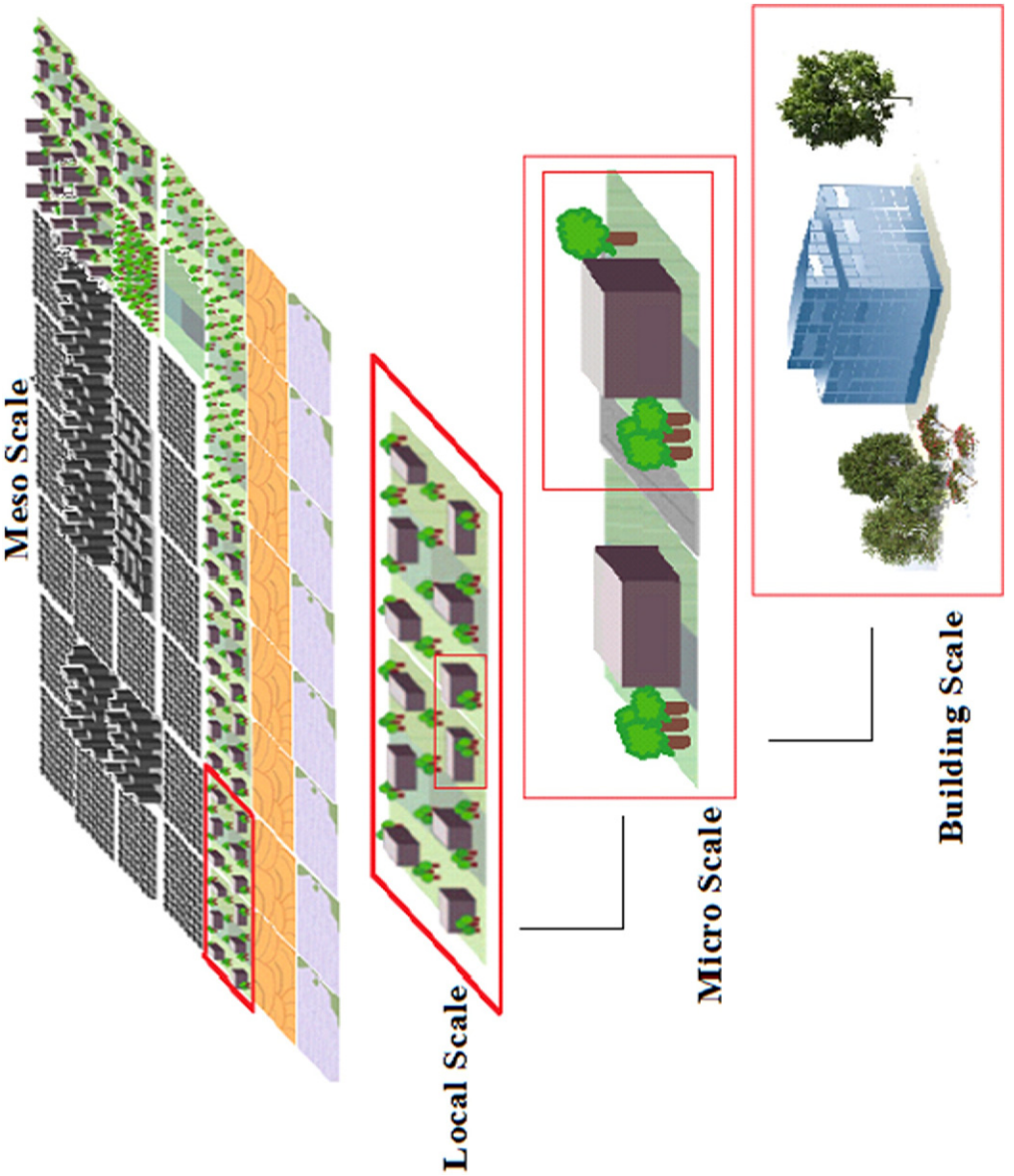
Meso Scale
Local Scale
Micro Scale
Building Scale

was span up until SMC reached an equilibrium and appropriate estimates of leaf area index were thus obtained for the initiation period (January 1st).

3.2. Test locations

Table 2 and Fig. 2 provide an overview of the four sites included in this work. SUEWS has mostly been applied in temperate climates though the simpler model LUMPS has been applied in arid environments before (Middel et al., 2012). Here we applied SUEWS to a newly (<2 years) instrumented site in Dublin, Ireland; a long term (5–10 years) site in Hamburg; Germany; a long term site in Melbourne, Australia; and an established site (2–4 years) in Phoenix, USA. The latter two sites represent environments with low precipitation and high annual temperatures, whereas the former two represent (i) a cool temperate climate with little annual temperature variation and high precipitation and (ii) a warm humid continental climate respectively. In Table 3, we highlight the required fractional values of land cover types required by SUEWS as computed using high resolution data and the LCZ approach.

The first site, Dublin Ireland – DUB – the flux observations are made on a mast located in a recently instrumented flat rooftop located on the grounds of a technical institute, just south of the centre of the urban area amidst a mix of dense commercial units and residential apartments (Sunderland et al., 2013; Keogh, 2015). The buildings surrounding the flux site are between 15 and 20 m tall, compact spacing with little vegetation. The site was not present during the initial test case of the LCZ-SUEWS approach in Dublin (Alexander et al., 2015). The synoptic station for DUB is located approximate 15 km north of the urban centre adjacent Dublin International Airport conforming to WMO standards; large homogenous fetch of short grass, no tall trees, and no nearby buildings.

The second site, Hamburg Germany – HAM – the flux observations are made at various height levels of a large telecommunications mast located 8 km east of the urban centre (Brümmer et al., 2012). This site essentially straddles two differing LCZs, to the west of the flux site, is characterised by large warehousing units < 15 m tall with little vegetation. To the East of the mast there is largely green vegetation, trees and little building coverage. The synoptic station for HAM is located at Hamburg International Airport approximately 11 km north of the urban centre, again conforming to WMO standards.

The third site, Melbourne Australia – MEL – here the flux observations are made in Preston, a suburban area located approximately 10 km north of the centre of Melbourne (Coutts et al., 2007). The instruments are located on a mast surrounded by medium density residential houses 5–8 m tall, open spacing and an ample amount of vegetation both grass and trees. The accompanying synoptic data were obtained from Melbourne Airport, located 23 km north-west of the urban centre.

The final site, Phoenix USA – PHX – for this location, observations are made within a residential area located 7.5 km North-West of downtown Phoenix in the suburban area of Maryvale (Chow et al., 2014). The surrounding area is comprised almost entirely of low rise residential housing 5-8 m tall with dry xeric landscaping i.e. little green vegetation. The synoptic data for this site were obtained from Phoenix Skyharbor airport which is proximate to the centre of the urban area (approximately 3.5 km southeast of downtown Phoenix). Solar radiation data were unavailable at Skyharbor airport, therefore solar radiation data for a nearby Arizona Meteorological network (AZMET) station located 1 km northwest of the airport at Encanto were used.

Fig. 3 provides annual wind roses from each location based on the flux data, Fig. 4 shows LCZ descriptions applicable immediately below and surrounding each of the sites along with satellite imagery. These LCZ descriptions (along with wind direction) were used to filter the observational data to ensure the source area for each site was consistent with the LCZ type used for the model runs. For example, for DUB site, this meant including westerly vectors while excluding easterly winds. For HAM, observational data were split into 2 sub datasets corresponding with LCZ 8 (westerly flows) and LCZ D (easterly flows). For the purposes of this study we only considered the LCZ 8 data for the Hamburg site. For both MEL and PHX the relative

Fig. 1. LCZ-SUEWS approach: At the mesoscale (10s–100s of km^2), model parameters are derived by integrating all LCZ across the entire domain. At the local scale (1–10s of km^2) specific model parameters for **individual** LCZ types are derived. At the microscale and building scale (10s–100s of m^2) the approach is as yet untested, but would involve the addition of building dimensions and spacing, individual vegetative species as well as detailed material data.

Table 1
Outline of systematic experiment used to test the LCZ-SUEWS approach across multiple sites/climates/urban configurations. Each stage subsequent to stage 1 adds additional detail, hence, when interpreting results, the additional effort in providing these data should be considered.

Stage	Experiment alias	Land cover data use for model run	Meteorological data used for model run
1	Base-line	Local climate zone fractions derived from sampling sites across the urban area	Proximate WMO standard synoptic station (airport sites): T, RH, K↓, Pr, P, U, V
2	Detailed land cover	Fractional values derived from 1 km^2 immediately surrounding flux site	Proximate WMO standard synoptic station (airport sites): T, RH, K↓, Pr, P, U, V
3	Detailed meteorology	Fractional values derived from 1 km^2 immediately surrounding flux site	Meteorological data collected adjacent flux observation platforms: T, RH, K↓, L↓, Pr, P, U, V

homogeneity of the surrounding urban area (along with the low wind speeds) meant no additional filtering was carried out on the provided observational data.

3.3. Evaluation of experiments

The performance of SUEWS run in each stage of the experiment is evaluated against the observations at each of the sites. Table 4 highlights the observational data available against which the model is judged, Table 5 highlights the raw data post-processing steps undertaken at each site along with the instruments used at each site. We employed root mean squared error (RMSE) and mean fractional bias (MFB) and Taylor diagrams which further employ the centred RMSE (E′), the correlation coefficient (R), and the standard deviation (σ) (Taylor, 2001) to assess the model performance in each of the stages highlighted previously. Additionally, regression analysis was carried out between model simulations and observations, for this the coefficient of determination (R^2) is reported. For comparing seasonal model performance across stages, the RMSE is normalised (nRMSE) using a normalisation factor, which is computed using the difference between the maximum and minimum observed values (Shcherbakov et al., 2013).

4. Results

In the following sections the results of the systematic experiment for the four flux sites across each of the stages are presented. The differences in model performance between stages and how these differences related across the four sites is the primary focus. The performance of SUEWS in simulating the radiative fluxes where they have direct bearing on the subsequent estimation of the turbulent fluxes is also highlighted. Our analysis focused on two key temporal scales; (i) hourly/mean diurnal simulations and (ii) daily flux densities. We also examined seasonal performance focusing on two key periods where solar insolation is at a minimum / maximum and where phenological conditions result in different surface processes occurring, namely (i) winter-time, conventionally defined as the months of December January and February (DJF) in the northern hemisphere and (ii) summer-time, defined as June July and August (JJA). When reporting seasonal results, the months of DJF are used for MEL for summer and JJA for winter.

Table 2
Meta-data of the sites included in this study. Shown is the year in which observations were obtained, the background climate type, the location of both the flux sites and alternative synoptic stations. Shown also in meters are the instrument height of the flux towers (Z_m) the displacement height (Z_0) and the mean building height surrounding the site (Z_b).

Location	Year	Köppen	Site	LAT	LONG	WMO ID	Z_m	Z_0	Z_b
Dublin, Ireland	2013	Cfb	Flux	53.34	−6.27	–	37	0.6	16.3
Site code: DUB			Synoptic	53.43	−6.25	39690			
Hamburg, Germany	2014	Dfb	Flux	53.52	10.10	–	50	0.6	8.8
Site code: HAM			Synoptic	53.63	10.00	101470			
Melbourne, Australia	2004	Cfb	Flux	−37.73	145.01	–	40	0.4	6.4
Site code: MEL			Synoptic	−37.67	144.83	948660			
Phoenix, USA	2012	BWh	Flux	33.48	−112.14	–	22.1	0.5	4.5
Site code: PHX			Synoptic	33.42	−112.02	722780			

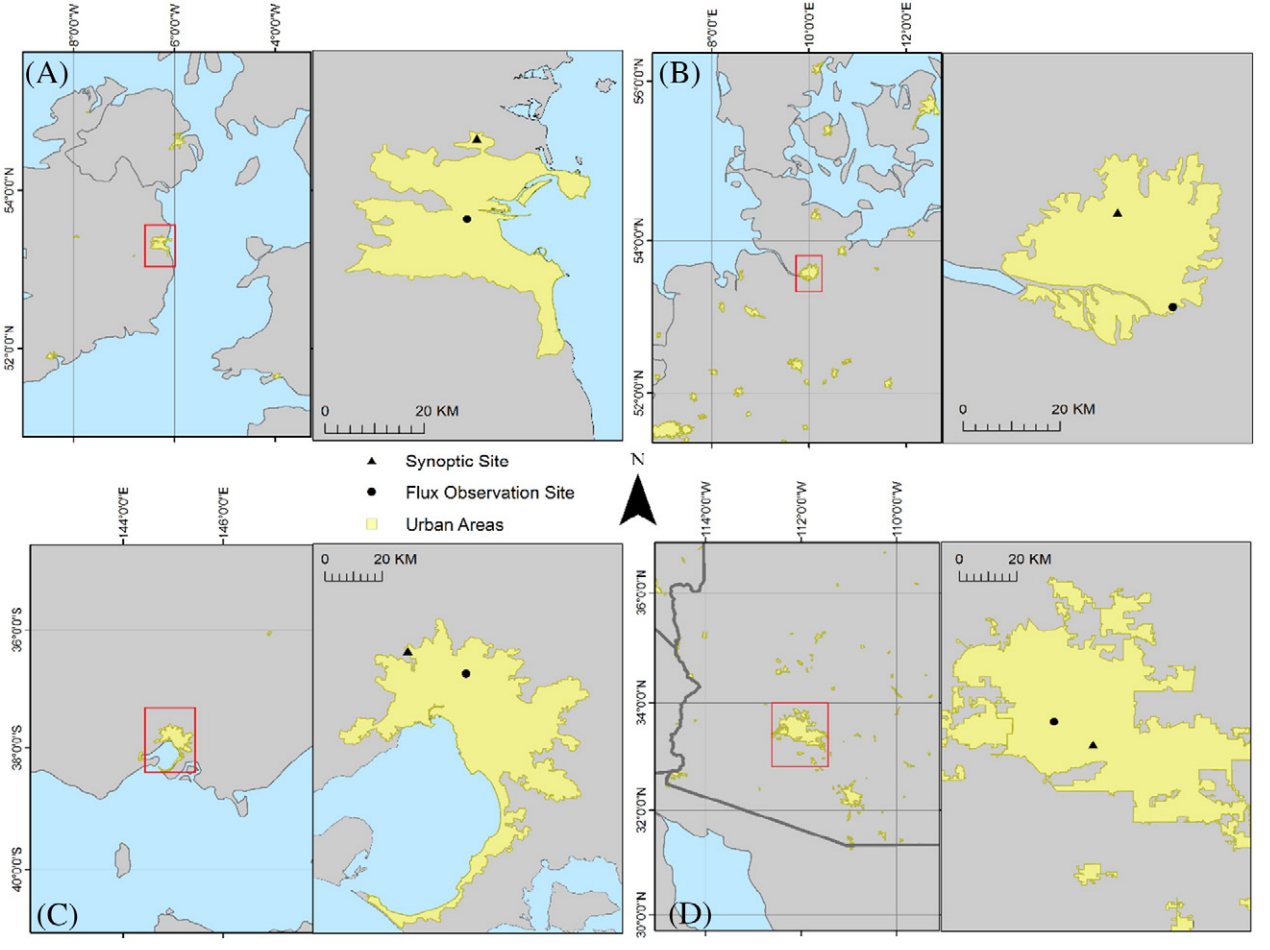

Fig. 2. Location of the four sites used in this experiment (A) is Dublin, Ireland (B) is Hamburg, Germany (C) is Melbourne, Australia (D) is Phoenix, USA. Shown are the locations of the synoptic and flux sites. Urban land cover obtained from Global Rural-Urban Mapping Project, Version 1 (GRUMPv1).

Table 3
Land cover fractions (λ) used to force the model calculated using the LCZ approach (stage 1) and traditional approach using high resolution (HR) data immediately surrounding the sites (stages 2 and 3).

Location	Land cover	Building	Pavements	Unmanaged	Trees	Grass	Water
Dublin, Ireland [DUB]	LCZ 2 - compact midrise	33	55	00	06	06	0
	HR[a]	39	49	00	10	02	0
Hamburg, Germany [HAM]	LCZ 8 - large low-rise	40	20	10	17	11	2
	LCZ D[b] - low plants	05	02	07	35	49	2
	HR[a]	27	15	07	22	18	11
Melbourne, Australia [MEL]	LCZ 6 - openset low-rise	37	16	0	21	26	0
	HR[c]	44	16	0	29	11	0
Phoenix, USA [PHX]	LCZ 6 - openset low-rise	49	18	27	02	04	0
	HR[d]	26	22	37	05	10	0

[a] Based on 1 km immediately surrounding flux site, λ calculated using 2.5 m imagery in Google Earth Pro™.
[b] Data not used in this study.
[c] Based on values reported in Coutts et al. (2007).
[d] Based on values reported in Chow et al. (2014).

4.1. Stage 1: daily and hourly performance results

The first stage of the experiment established a base-line performance against which the subsequent addition of more detailed meteorological and land cover data is judged. In this stage of the experiment, land cover data are not obtained directly from the area surrounding each of the flux sites, but rather by sampling the LCZ. The performance for each of the sites is highlighted in Table 6.

The ranking from lowest to highest RMSE (values reported in parenthesis) based on the daily estimates of Q_E-PHX performed best in stage 1 (9.66 W m^{-2}), followed by DUB (9.98 W m^{-2}), MEL (30.99 W m^{-2}) and HAM (37.72 W m^{-2}). In terms of model bias, PHX and MEL underestimate Q_E (−1.02, −0.18 respectively).

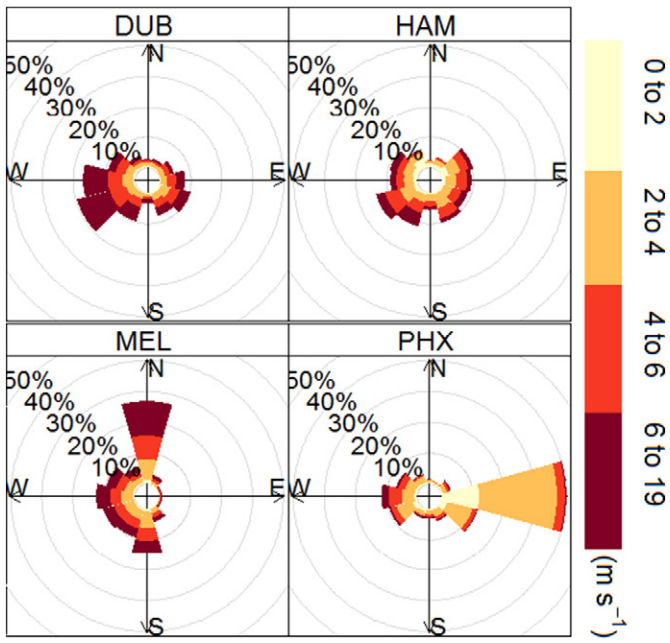

Fig. 3. Annual wind roses collected at the flux sites, each coloured bar represents a different wind speed (m s^{-1}), wind direction was partitioned into16 (22.5°) compass vectors.

Fig. 4. Top: Conceptual LCZ description of the land cover immediately surrounding each flux site. Bottom: Satellite imagery surrounding each of the sites (~500 × 500 m) from Google Earth Pro©.

Table 4
Descriptive statistics illustrating the availability of flux data (top rows) as a percentage of the entire year considered. Note: DOY 1 = -January 1st. Also given are the means (μ) and standard deviations (σ) of wind speed (u) relative humidity (rh) air temperature (Tair) air pressure (pres) and insolation (kdown) recorded at the synoptic sites. For precipitation (rain), the maximum hourly value recorded is given along with the annual sum.

	Site	DUB	$HAM_{LCZ\ 8}$	MEL	PHX
	Year	2013	2014	2004	2012
	DOY span	1–109, 149–305	1–365	1–70, 87–183, 210–242, 275–333	1–77, 108–110, 121–157, 164–223, 242–366
	N (valid)	3567 (45%)	4536 (57%)	3705 (47%)	6784 (86%)
U	μ	5.6	4.2	5.3	1.1
[m s^{-1}]	σ	2.9	2.1	2.8	0.9
RH	μ	81.7	80.7	67.5	28.2
[%]	σ	12.3	15.4	18.8	16.8
Tair	μ	9.5	10.8	13.7	25.1
[°C]	σ	5.5	7	5.3	9.3
pres	μ	101.4	101.4	101.6	101.1
[kPa]	σ	1.2	0.8	1.7	1.2
rain	Max	12.9	14.9	8.5	14.7
[mm]	Sum	763.9	679.4	448.6	114.19
kdown	μ	115.1	121	164.38	231.49
[W m^{-2}]	σ	188.2	197.7	253.29	308.92

DUB and HAM both showed negligible negative and positive biases (−0.02 and 0.02) respectively. For Q_H the ranking from lowest to highest daily RMSE values was DUB (24.65 W m^{-2}) HAM (32.07 W m^{-2}) MEL (32.31 W m^{-2}) and PHX (47.27 W m^{-2}) in stage 1. Q_H was underestimated for the DUB site (−0.16) and overestimated for HAM (0.67), MEL (0.62) and PHX (0.31).

For Q_E the highest R^2 value achieved in stage 1 was for HAM the lowest value was for PHX followed by MEL and DUB. Q_H in stage 1 is characterised by relatively high R^2 values compared to Q_E (ranging from 0.26 to 0.69).

The calculation of RMSE based on hourly values often includes large isolated errors which can occur between specific hourly flux densities, these errors can arise either due to observational errors which were not filtered correctly or poor model performance. Unsurprisingly for most sites/variables, hourly RMSE was higher than daily RMSE, for instance, for DUB Q_E RMSE was 37.11 W m^{-2} which was approximately 3.5 times higher (i.e. worse) than the daily performance, though this was an extreme example. Generally hourly performance was 1.5 times poorer than daily for Q_E and Q_H in stage 1.

4.1.1. Stage 2 and stage 3: performance results

In the second stage of the experiment, the land cover types used for the model runs were modified using fractional values calculated out to 1 km^2 surrounding each site. While these fractional values relate to the area directly surrounding the flux site, they require additional effort to compute. The largest difference between stages 1 and 2 in terms of land cover fractions was HAM and PHX which both had significantly lower building fractions than those calculated using the LCZ approach – recall Table 3. This was borne out in the model performance – Table 6. The impact of high resolution land cover was to increase daily RMSE marginally for Q_E at all sites. The largest RMSE increase was 9.3 W m^{-2} compared to stage 1 for HAM, followed by PHX, RMSE increased by 3.5 W m^{-2}. The increase was 0.53 W m^{-2} and 1.71 W m^{-2} for DUB and MEL respectively. The impact on daily Q_H was less consistent across the sites compared to Q_E. For MEL and PHX a slight improvement was seen (RMSE decreased by 0.54 and 4.77 W m^{-2} respectively) whereas performance decreased slightly for DUB (0.83 W m^{-2}) and HAM (6.89 W m^{-2}).

Model bias did not change direction in stage 2, for HAM the positive bias (i.e. model overestimation) for Q_E increased by 0.18. For MEL and PHX, which both exhibited negative bias (i.e. model underestimation) in stage 1 also had negative biases in stage 2. The bias increased by 0.17 for MEL but a significant improvement was seen in PHX, bias was reduced by 0.22, though the model still underestimated Q_E. For DUB, there was no change in bias for Q_E and Q_H between stages 1 and 2. Interestingly, the impact on RMSE calculated from the hourly flux densities in stage 2 was an average reduction in RMSE of 2.5 W m^{-2}. The largest improvement in hourly flux calculation was Q_E for DUB which reduced RMSE by 15.57 W m^{-2}.

Table 5
Meta-data illustrating instrumentation at the four flux site along with corrections carried out on flux measurements.

	Site			
	DUB	HAM	MEL	PHX
Instruments [model]	Tower (48 m AGL) • 3D sonic anemometer [WindMaster Pro, Gill] • Gas analyser [LI-7200] • Temperature-relative humidity sensor [HMP45C] • Net radiometer [NR-01] 47 m Roof level (37 m) • Tipping bucket rain gauge [ARG100]	Tower (50 m AGL) • 3D sonic anemometer [USA-1] • Gas analyser [LI-7500] • Thermometer [Pt-100] • Humidity sensor [HMP 45] 12 m • Pyranometer [Kipp + Zonen] • Pyrgeometer [Eppley] Ground level • Pressure sensor [PTB 200 A] • Tipping bucket rain gauge	Tower (40 m AGL) • 3D sonic anemometer [CSAT3] • Infrared gas analyser [LI-7500] • Krypton hygrometer [KH20] • Temperature-relative humidity [HMP45C] • Net radiometer [Q7.1] • Albedometer [CM 7B] • Pyrgeometer [CG2]	Tower (22 m AGL) • 3D sonic anemometer [CSAT3] • Infrared gas analyser [LI-7500] • Temperature-relative humidity sensor [HMP45AC] • Net radiometer [NR-01] Ground level • Rain gauge [TB4]
10/20 Hz data corrections	1. Planar fit rotation (Wilczak et al., 2001) 2. Block averaged (30 min) 3. Offset for sensor lag (co-variance maximization) 4. Signal de-spiking (Vickers and Mahrt, 1997), accepted spikes: 1% 5. Missing sample allowance 10% 6. Density effects (Webb et al., 1980) 7. Flagging according Foken 2003, QC ≥ 7 discarded Foot print model: Kormann and Meixner, 2001	1. Double rotation 2. Block averaged (60 min) 3. Offset for sensor lag (co-variance maximization) 4. Signal de-spiking (Mauder et al., 2013), accepted spikes: 2% 5. Missing sample allowance 10% 6. Density effects (Webb et al., 1980) 7. Flagging according Foken 2003, QC ≥ 7 discarded Foot print model: Kormann and Meixner, 2001	1. Signal de-spiking 2. Oxygen absorption (Tanner et al., 1993) 3. Offset for sensor lag 4. Block averaged (30 min) 5. Density effects (Webb et al., 1980) Foot print model: None reported	1. Signal de-spiking 2. Aligned into natural wind coordinates (w = 0) (Kaimal & Finnigan, 1994) 3. Offset for sensor lag 4. Block averaged (30 min) 5. Frequency response correction 6. Density effects (Webb et al., 1980) Foot print model: Schmid et al., 1991

Table 6
Root Mean Square Error (RMSE) statistics (W m^{-2}) calculated for daily mean flux density and individual hourly flux densities. Also shown are mean fractional bias (MFB) calculated using the daily flux densities (−2 to +2). Also shown is the coefficient of determination (R^2). Below presents a colour key summary for highest and lowest daily RMSE scores illustrating the best performance (lowest RMSE) to worse performance (highest RMSE): Lowest RMSE (best performance) = green, highest RMSE (worst performance) = red, intermediate RMSE = yellow.

	[DUB]				[HAM]				[MEL]				[PHX]			
	Q_E															
Stage	R^2	RMSE	RMSE (hourly)	MFB	R^2	RMSE	RMSE (hourly)	MFB	R^2	RMSE	RMSE (hourly)	MFB	R^2	RMSE	RMSE (hourly)	MFB
1	0.11	9.98	37.11	-0.02	0.45	37.72	23.96	0.02	0.06	30.99	26.11	-0.18	0.01	9.66	20.91	-1.02
2	0.10	10.51	21.54	0.01	0.48	47.02	27.78	0.20	0.07	32.70	25.75	-0.35	0.06	13.16	21.40	-0.80
3	0.06	19.47	25.79	0.67	0.47	51.53	48.81	0.17	0.05	32.67	23.55	-0.46	0.00	7.99	21.43	-1.26
	Q_H															
Stage	R^2	RMSE	RMSE (hourly)	MFB	R^2	RMSE	RMSE (hourly)	MFB	R^2	RMSE	RMSE (hourly)	MFB	R^2	RMSE	RMSE (hourly)	MFB
1	0.67	24.65	28.61	-0.16	0.56	32.07	43.51	0.67	0.26	32.31	49.36	0.62	0.69	47.27	65.38	0.31
2	0.67	25.48	25.41	-0.17	0.54	38.96	37.87	0.58	0.25	31.77	52.39	0.69	0.67	43.59	60.40	0.27
3	0.59	39.89	32.68	-0.74	0.57	40.74	59.48	0.61	0.31	33.66	41.89	0.48	0.79	45.37	61.32	0.46
n		128	3567			353	4536			235	3705			291	6784	

Table 7
Seasonal RMSE values calculated for each site. Summer refers to June July and August for DUB, HAM and PHX and December January February for MEL. Winter refers to December January February for DUB, HAM and PHX and June July and August for MEL. RMSE values are in W m^{-2}. RMSE values are derived using daily flux densities thus are slightly more conservative than hourly RMSE values. Given also is the nRMSE which normalises the RMSE using the range of observational data, hence the effect of larger flux magnitudes in summer are removed. Highlighted are values where the mean observed flux density was close to 0 W m^{-2} meaning the normalised values should be interpreted with caution.

Q_E						Q_H					
Stage	Metric	DUB	HAM	MEL	PHX	Stage	Metric	DUB	HAM	MEL	PHX
Summer						Summer					
1	RMSE	12.13	27.69	16.08	29.27	1	RMSE	25.86	46.86	39.29	48.70
2	RMSE	12.75	26.76	17.05	22.46	2	RMSE	27.39	35.22	40.89	39.65
3	RMSE	18.09	25.98	16.84	31.40	3	RMSE	28.85	31.74	34.37	57.04
1	nRMSE	51.7%	22.9%	24.1%	23.0%	1	nRMSE	16.7%	36.7%	20.9%	32.3%
2	nRMSE	54.4%	22.1%	25.6%	17.6%	2	nRMSE	17.7%	27.6%	21.8%	26.3%
3	nRMSE	77.1%	21.5%	25.2%	24.6%	3	nRMSE	18.6%	24.8%	18.3%	37.8%
Winter						Winter					
1	RMSE	8.28	10.78	20.39	13.32	1	RMSE	23.05	21.93	39.92	17.59
2	RMSE	8.73	12.08	20.38	18.71	2	RMSE	25.40	22.87	44.31	20.82
3	RMSE	21.42	41.36	19.90	13.65	3	RMSE	41.85	48.32	24.44	23.47
1	nRMSE	21.4%	19.6%	16.7%	84.8%	1	nRMSE	15.2%	19.9%	38.4%	24.3%
2	nRMSE	22.6%	21.9%	18.3%	119.1%	2	nRMSE	16.7%	20.8%	42.2%	28.8%
3	nRMSE	55.4%	75.1%	17.7%	86.9%	3	nRMSE	27.6%	43.9%	24.1%	32.5%

For the final stage of the experiment, off-site meteorological forcing data was replaced with measurements made on site. The most significant difference for this stage is the use of observations of the incident radiation (K↓, L↓) made at the four sites. There was little impact on daily RMSE in stage 3 for HAM, MEL and PHX when compared to values for stage 2. For DUB, daily RMSE increased by 8.96 and 14.41 W m^{-2} for Q_E and Q_H respectively. For HAM, RMSE increased by 4.51 and 1.78 W m^{-2} for Q_E and Q_H, whereas for PHX, RMSE was decreased by 5.17 W m^{-2} for Q_E and increased by 1.78 W m^{-2} for Q_H. RMSE for MEL was practically unchanged in terms of Q_E between stages 2 and 3 (improved model performance by 0.03 W m^{-2}) similarly to HAM and PHX the difference in Q_H was <2 W m^{-2} (1.89 W m^{-2}).

A larger impact was seen in the hourly flux density RMSE, particularly for HAM - moving from stages 2 to 3, RMSE increased by a similar amount for both Q_E (21.03 W m^{-2}) and Q_H (21.61 W m^{-2}) though the bias remained positive indicating overestimation by the model compared to the observations. For DUB, model RMSE also increased between stages 2 and 3 by 4.25 and 7.27 W m^{-2} for Q_E and Q_H. For MEL, hourly performance improved (RMSE decreased) slightly for Q_E (2.2 W m^{-2}) and Q_H (10.5 W m^{-2}) between stages 2 and 3. There was no impact on hourly RMSE for PHX between stages 2 and 3 (0.03 and 0.92 W m^{-2}) – though it should be noted hourly Q_H RMSE was the highest amongst the four sites with a persistent positive bias (model over estimation of Q_H compared to observations).

4.2. Seasonal and annual performance results

The seasonal RMSE values are given in Table 7. Model performance tended to be better in winter than summer for all sites during all stages based on the RMSE. RMSE for Q_E was lower than Q_H for all sites in both seasons. Looking initially at difference between the seasonal RMSE for individual stages, the largest difference in model performance was for Q_H for PHX, performance in summer was 31.11, 18.83 and 33.57 W m^{-2} worse than winter in stages 1, 2 and 3 respectively. The smallest difference in seasonal performance was for Q_E for DUB.

Examining the seasonal difference across all stages reinforces the trend between summer and winter performance. The performance in summer is worse for both Q_H and Q_E, the exception was Q_E for MEL which exhibits higher RMSE in winter and Q_H for DUB which was slightly higher, though this was due to large wintertime RMSE in stage 3: for stage 1 and 2 RMSE was higher in summer. While there was a clear difference in the seasonal performance for all sites, the difference between stages were small with only some exceptions.

To account for the seasonal differences in the magnitude of available energy between winter and summer and enable comparison across seasons, the nRMSE was also calculated, which normalises the RMSE using the range of observed turbulent flux magnitude. This relates the magnitude of the error to the magnitude of the observed flux. Where the mean of the observed flux approaches 0 W m^{-2} (values highlighted in Table 7) the nRMSE should be interpreted with some caution. Nevertheless, nRMSE for Q_E and Q_H tended to be lower in winter than summer for stages 1-2.

The overall annual performance for each of the sites is presented as Taylor diagrams in Fig. 5, which compares the individual stages. Taking the entire annual performance across all sites, the difference between stages 1 and 2 is generally lower than between stages 1 and 3. The centred RMSE for Q_H tended to be slightly higher for all sites, there was also stronger correlation with observations for Q_H than for Q_E. The simulated annual variation (σ) across the entire period was close with the variation in observations, the clear exceptions were Q_E for DUB which exhibited significant higher variation in observations compared to the model in all stages. The other exception was Q_H for MEL which illustrated higher variation in the model compared with the observations. Stage 1 (LCZ derived inputs) and stage 2 (high-resolution land cover) exhibited similar performances on an annual basis.

5. Discussion

Despite differences in background climate, urban land cover type, building materials, and vegetative species, the performance of SUEWS in simulating the turbulent fluxes Q_E and Q_H is broadly consistent between sites. RMSE for Q_E falls into a range of between 20 and 30 W m^{-2} while a RMSE range of 40–60 W m^{-2} for Q_H captures all sites, ranges similar to those reported in Järvi et al. (2011) for Los Angeles and Vancouver. The improved ability of the model in simulating Q_E is evident, errors were consistently lower than Q_H for most of the sites.

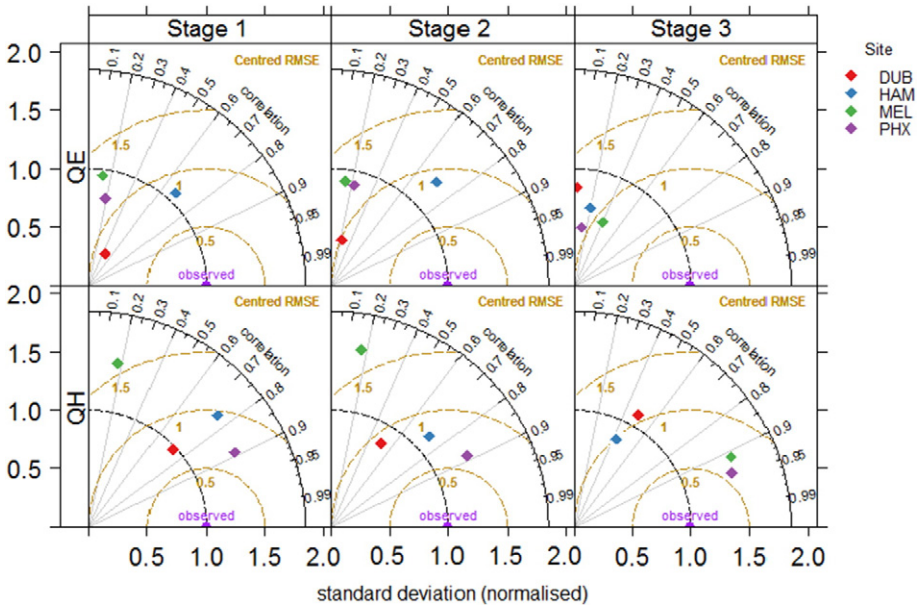

Fig. 5. Taylor diagrams based on all (i.e. hourly) observations for Q_E (top panels) and Q_H (bottom panels). Data have been normalised using observations to allow comparisons between sites and stages, hence, RMSE magnitude is expressed in standard deviations compared to observed data.

The addition of high resolution land cover fractions did not significantly impact on model performance across any of the sites considered, despite large differences between those calculated by the LCZ approach. Given the increased amount of effort required to derive the high resolution fractions, it appears LCZ fractional values can satisfactorily be used in combination with the SUEWS model.

In all stages, the model captures well the relative differences between the four sites when considering both latitude and urban density. For the urban LCZ considered here, $Q_H > Q_E$ while Q_E is higher in summer owing to phenological development and higher amount of energy. Both of these factors may explain the seasonal variation in performance whereby performance was better in winter than summer. Vegetation, even small amounts, have been identified as a critical component for most UEB models (Loridan et al., 2010; Grimmond et al., 2011), here single species (i.e. deciduous or coniferous) were used for all sites, it is possible that increased detail on annual phenological development, observed LAI progression for example, along with multiple species will reduce the seasonal differences in model performance.

As different levels of data are added to the model for the experiment, the impact on performance relative to the observation sites was broadly consistent across all domains. In terms of hourly simulations of Q_H, using additional details on surrounding land cover fractions improved the model performance, though the reduction in RMSE was relatively minor (often <15 W m^{-2}) compared to stage 1 - there was no impact on bias direction. Similar magnitudes were found in previous work.

The impact of adding meteorological data collected adjacent the flux sites is the most difficult finding to explain. Generally, performance was diminished using on-site meteorological data coupled with high resolution land cover in all cases except PHX, though the differences were extremely small. This may be due to observational error whereby the meteorological data collected alongside the towers are unduly influenced by local effects whereas the flux platforms themselves have a more representative fetch. This would certainly be the case for DUB and HAM which had relatively heterogeneous fetches surrounding the flux sites.

As with previous studies, errors should not be attributed solely to model performance; observations of Q_E are notoriously difficult and subject to large errors/uncertainty particularly immediately during and after precipitation events. Observations at each of the flux sites included underwent post processing of some kind however some observational errors may have been included despite this and despite the additional filtering carried out using the LCZ approach and wind vectors. For instance, the magnitude of observed Q_E for DUB [LCZ

2] was larger than would be expected given the sparse amount vegetation surrounding this site. A similarly instrumented site also classed as LCZ 2 (reported in Alexander et al., 2015) exhibited a much lower magnitude and range of Q_E during summer months, where the maximum observed value was about 60 W m^{-2} and a median value of 25 W m^{-2}. Here, the observed median value for DUB during summer was 67.57 W m^{-2} with a maximum of 215 W m^{-2} around midday. There is nothing that readily accounts for the large magnitude of Q_E observed at this site, again given the lack of vegetation. The instruments for DUB are located about 5 m lower than the alternative LCZ 2 site, so it is unlikely to be due to measurements being made within the roughness sublayer. However, this only occurred for the diurnal profiles, averaging over multiple hours and days goes some ways towards filtering out such erroneous observations. In terms of the HAM site, the addition of more detailed land cover data resulted in a decrease in model performance – this is likely attributed to the source area of the observations following the filtering process. Note the fractional values immediately surrounding the site have a higher fraction of vegetation and water coverage however the observational dataset sought to exclude the influence of these land cover types. It is unsurprising the model overestimated the magnitude of Q_E in this instance.

Another important component for UEB model performance is net radiation. Here, there was a consistent overestimation of Q_H for PHX, this was due to the model underestimation of albedo (α) leading to lower value of K↑ (not shown). The model estimated α to be 0.15 – however in reality, the building material in PHX are much lighter than the group average, as such, α based on observations was ~0.25. Therefore, the model retained more energy, leading to overestimation of both Q_E and Q_H. This means a subset of LCZ material properties may need to be compiled for applying the model in environments with similar building materials, but it should be noted the partitioning of energy normalised by available energy, that is Q_H/Q^* and Q_E/Q^*, was similar between observations and the modelled fluxes.

Nevertheless, SUEWS simulations for both daily and hourly turbulent fluxes agree well with observations using the LCZ approach, with errors well within previously reported ranges. This enables us for the first time to carry out inter-site comparisons in the UEB across similar LCZ types. Fig. 6 shows the diurnal flux profiles for three LCZ 6 sites (derived using the setup in stage 1) to illustrate this point. As shown, the partitioning of energy amongst these sites is remarkably similar. Day length (i.e. positive Q*) is shown to be slightly longer in the DUB data with a lower amount of energy at midday as would be expected of this climate. As a consequence, Q* at midday was 457.25 W m^{-2}, 65 W m^{-2} lower than MEL and 132 W m^{-2} lower than PHX.

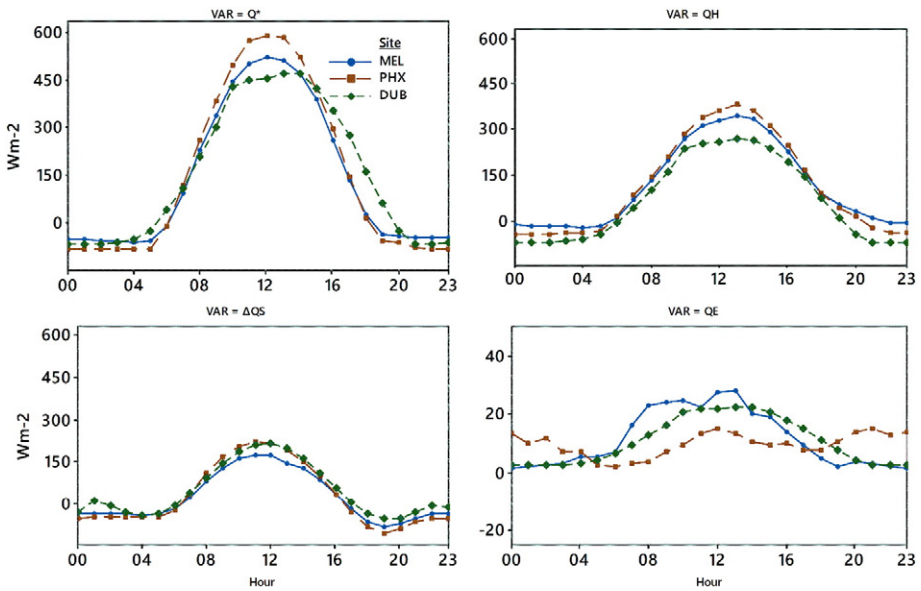

Fig. 6. LCZ 6 summer time Diurnal profile for MEL, PHX and also shown is LCZ 6 site for DUB as presented in Keogh et al. (2012) and Alexander et al. (2015) Top left panel is Q*, followed by Q_H (top right), ΔQ_S (bottom left) and Q_E (bottom right).

PHX exhibits slightly higher proportion of energy expended towards Q_H throughout the course of the day compared to both DUB and MEL, as would be expected given the lack of vegetation/water in this environment. The differences in land cover can also be examined e.g. building material and artificial surface extent across all sites can be examined in detail to explore the effect on ΔQ_S – a principle component of nocturnal UHI formation.

The use of a standardised method for collecting land cover (LCZ) and meteorological data in order to preform initial assessments of an area's urban energy and water balance should not discourage the continued establishment of high-quality and long-term flux towers in cities. Here, we considered only three LCZ classes, namely LCZ 2, 6 and 8 as these represented the sites with available data. As additional instrumented sites become available, the approach outlined here should undergo further evaluation.

While the approach has obvious applications in overcoming fiscal/computational limitations in cities with limited resources, the application of the approach needs to be further validated in sparse urban environments, as well as non-urban environments. Different background climates should also be considered. While we requested urban flux data for a range of background climates the four sites included in this study were the only cities for which data were made available. Therefore, eddy-covariance platforms are still an essential investment in any city. Despite the limited sites included here, the extension of the LCZ-SUEWS approach into additional arid/continental type climates undertaken here builds upon the original case study, which further supports the notion that the approach employed with the SUEWS model is capable of realistically simulating the UEB in a variety of circumstances and urban environments.

6. Conclusions

In this study we systematically tested a modeling approach which seeks to overcome data scarcity in terms of urban morphology and meteorological observations made within the urban environment. To that end, we coupled the local climate zone (LCZ) scheme of Stewart and Oke (2012) with the surface energy and water balance scheme (SUEWS) v.2014b (Järvi et al., 2014). The approach was tested in four background climates and different urban configurations. Detailed land cover data and meteorological observations were added to the SUEWS model in stages to examine the impact on model performance relative to the coarse LCZ data and meteorological observations made at airports conforming to WMO standards.

The results show that the addition of detailed data on model performance varied across the sites considered, however root mean squared error (RMSE) consistently fell within a range of between 20 and 40 W m^{-2} for Q_E and between 40 and 60 W m^{-2} for Q_H. The difference between the use of LCZ and detailed land cover was generally small indicating that utilising LCZ data with SUEWS for the initial assessment of the urban energy and water balance is an appropriate approach to take. Furthermore, meteorological observations which are designed to exclude the urban effect are appropriate as forcing data for SUEWS, without impacting significantly on model performance. The results indicate that this modeling approach can be used in data poor settings to rapidly derive in a consistent manner the parameters required by most urban climate models, provided an LCZ map of the city is available.

Acknowledgements

The authors wish to thank Dr. Andrew Coutts and Prof. Sue Grimmond for kindly providing the data for Melbourne. We also wish to thank Prof. Anthony Brazel for providing the synoptic data for Phoenix. We thank Dr. Stephanie Keogh for providing the flux data for Dublin, and for her advice on various post-processing techniques. We thank the Meteorological Institute of the University of Hamburg and especially Ingo Lange, Felix Ament and Marvin Heidkamp for providing the Hamburg Weather Mast data and for their support. The Dublin flux towers are funded by the Higher Education Authority (HEA) of Ireland. The Phoenix flux tower is funded by National Science Foundation grants BCS-1026865, DEB-0423704, DEB-9714833, ATM-0710631, CNH-0814692, NUS-R-109-000-162-133, and Earth Systems Models (EaSM) Program Award #1049251.

References

Alexander, P., Mills, G., 2014. Local climate classification and Dublin's urban heat island. Atmosphere 5 (4), 755–774.
Alexander, P., Mills, G., Fealy, R., 2015. Using LCZ data to run an urban energy balance model. Urban Climate 13 (3), 14–37.

Ali-Toudert, F., Mayer, H., 2006. Numerical study on the effects of aspect ratio and orientation of an urban street canyon on outdoor thermal comfort in hot and dry climate. Build. Environ. 41 (2), 94–108.
Allen, L., Lindberg, F., Grimmond, C., 2011. Global to city scale urban anthropogenic heat flux: model and variability. Int. J. Climatol. 31 (13), 1990–2005.
Atkinson, B., 2003. Numerical modelling of urban heat-island intensity. Bound.-Layer Meteorol. 109 (3), 285–310.
Barlow, J., Harman, I., Belcher, S., 2004. Scalar fluxes from urban street canyons. Part I: laboratory simulation. Bound.-Layer Meteorol. 113 (3), 369–385.
Bechtel, B., et al., 2015. Mapping local climate zones for a worldwide database of the form and function of cities. ISPRS Int. J. Geo-Inf. 4 (1), 199–219.
Block, A., Keuler, K., Schaller, E., 2004. Impacts of anthropogenic heat on regional climate patterns. Geophys. Res. Lett. 31 (12).
Bottyán, Z., Unger, J., 2003. A multiple linear statistical model for estimating the mean maximum urban heat island. Theor. Appl. Climatol. 75 (3), 233–243.
Brümmer, B., Lange, I., Konow, H., 2012. Atmospheric boundary layer measurements at the 280 m high Hamburg weather mast 1995–2011: mean annual and diurnal cycles. Meteorol. Z. 21 (4), 319–335.
Bueno, B., Norford, L., Hidalgo, J., Pigeon, G., 2013. The urban weather generator. J. Build. Perform. Simul. 6 (4), 269–281.
Ching, J., 2013. A perspective on urban canopy layer modeling for weather, climate and air quality applications. Urban Climate 3 (1), 13–39.
Chow, W., et al., 2014. Seasonal dynamics of a suburban energy balance in Phoenix, Arizona. Int. J. Climatol. 34 (15), 3863–3880.
Colunga, M., et al., 2015. The role of urban vegetation in temperature and heat island effects in Querétaro city, Mexico. Atmosfera 28 (3), 205–218.
Coutts, A., Beringer, J., Tapper, N., 2007. Impact of increasing urban density on local climate: spatial and temporal variations in the surface energy balance in Melbourne, Australia. J. Appl. Meteorol. Climatol. 46 (4), 477–493.
de Dear, R., Brager, G., 1998. Developing an Adaptive Model of Thermal Comfort and Preference. ASHRAE Transactions 104(1). Center for the Built Environment, pp. 1–18.
De Ridder, K., Lauwaet, D., Maiheu, B., 2015. UrbClim – a fast urban boundary layer climate model. Urban Climate 12 (June 2015), 21–48.
Dupont, S., Otte, T., Ching, J., 2004. Simulation of meteorological fields within and above urban and rural canopies with a mesoscale model. Bound.-Layer Meteorol. 113 (1), 111–158.
Eliasson, I., 2000. The use of climate knowledge in urban planning. Landsc. Urban Plan. 48 (1-2), 31–44.
Fan, H., Sailor, D., 2005. Modeling the impacts of anthropogenic heating on the urban climate of Philadelphia: a comparison of implementations in two PBL schemes. Atmos. Environ. 39 (1), 73–84.
Fenner, D., Meier, F., Scherer, D., Polze, A., 2014. Spatial and temporal air temperature variability in Berlin, Germany, during the years 2001–2010. Urban Climate 10 (2), 308–331.
Grimmond, C., Oke, T., 1991. An evaporation-interception model for urban areas. Water Resour. Res. 27 (7), 1739–1755.
Grimmond, C., Oke, T., 1999. Heat storage in urban areas: local-scale observations and evaluation of a simple model. J. Appl. Meteorol. 38 (2), 922–940.
Grimmond, C., Oke, T., 2002. Turbulent heat fluxes in urban areas: observations and a local-scale urban meteorological parameterization scheme (LUMPS). J. Appl. Meteorol. 41 (7), 792–810.
Grimmond, C., et al., 2010. The international urban energy balance models comparison project: first results from phase 1. J. Appl. Meteorol. Climatol. 49 (6), 1268–1292.
Grimmond, C., et al., 2011. Initial results from Phase 2 of the international urban energy balance model comparison. Int. J. Climatol. 31 (2), 244–272.
Harman, I., Belcher, S., 2006. The surface energy balance and boundary layer over urban street canyons. Q. J. R. Meteorol. Soc. 132 (621), 2749–2768.
Harman, I., Barlow, J., Belcher, S., 2004. Scalar fluxes from urban street canyons part II: model. Bound.-Layer Meteorol. 113 (3), 387–410.
Heaphy, L., 2015. The role of climate models in adaptation decision-making: the case of the UK climate projections 2009. Eur. J. Philos. Sci. 5 (2), 233–257.
Hebbert, M., Mackillop, F., 2013. Urban climatology applied to urban planning: a postwar knowledge circulation failure. Int. J. Urban Reg. Res. 37 (5), 1542–1558.
Hidalgo, J., et al., 2008. Advances in urban climate modeling. Ann. N. Y. Acad. Sci. 1146, 354–374.
Hoffmann, P., Krueger, O., Schlünzen, K., 2012. A statistical model for the urban heat island and its application to a climate change scenario. Int. J. Climatol. 32 (8), 1238–1248.
Huang, H., Akutsu, Y., Arai, M., Tamura, M., 2000. A two-dimensional air quality model in an urban street canyon: evaluation and sensitivity analysis. Atmos. Environ. 34 (5), 689–698.
Järvi, L., Grimmond, C., Christen, A., 2011. The Surface Urban Energy and Water Balance Scheme (SUEWS): evaluation in Los Angeles and Vancouver. J. Hydrol. 411 (3-4), 219–237.
Järvi, L., et al., 2014. Development of the Surface Urban Energy and Water Balance Scheme (SUEWS) for cold climate cities. Geosci. Model Dev. 7, 1691–1711.
Kaimal, J.C., Finnigan, J.J., 1994. Atmospheric boundary layer flows-Their structure and measurement. Oxford University Press 289 pp.
Karppinen, A., et al., 2000. A modelling system for predicting urban air pollution: comparison of model predictions with the data of an urban measurement network in Helsinki. Atmos. Environ. 34 (22), 3735–3743.
Keogh, S., 2015. Quantifying Carbon Dioxide Concentrations and Fluxes for Dublin. National University of Ireland Maynooth, Kildare, Ireland.
Keogh, S., Mills, G., Fealy, R., 2012. The energy budget of the urban surface: two locations in Dublin. Ir. Geogr. 4 (1), 1–23.
Kormann, R., Meixner, F.X., 2001. An analytical footprint model for non-neutral stratification. Bound.-Layer Meteorol. 99, 207–224. http://dx.doi.org/10.1023/A:1018991015119.
Kusaka, H., Kimura, F., 2004. Coupling a single-layer urban canopy model with a simple atmospheric model: impact on urban heat island simulation for an idealized case. J. Meteorol. Soc. Jpn. 82 (1), 67–80.
Leconte, F., Bouyer, J., Claverie, R., Pétrissans, M., 2015. Using Local Climate Zone scheme for UHI assessment: evaluation of the method using mobile measurements. Build. Environ. 83, 39–49.
Loridan, T., Grimmond, C., 2012. Multi-site evaluation of an urban land-surface model: intra-urban heterogeneity, seasonality and parameter complexity requirements. Q. J. R. Meteorol. Soc. 138 (665), 1094–1113.

Loridan, T., et al., 2010. Trade-offs and responsiveness of the single-layer urban canopy parametrization in WRF: an offline evaluation using the MOSCEM optimization algorithm and field observations. Q. J. R. Meteorol. Soc. 136 (649), 997–1019.
Masson, V., et al., 2014. Adapting cities to climate change: a systemic modelling approach. Urban Climate 10 (December 2014), 407–429.
Mauder, M., Cuntz, M., Drüe, C., Graf, A., Rebmann, C., Schmid, H.P., Scmidt, M., Steinbrecher, R., 2013. A strategy for quality and uncertainty assessment of long-term eddy-covariance measurements. Agric. For. Meteorol. 169, 122–135.
Middel, A., et al., 2012. Land cover, climate, and the summer surface energy balance in Phoenix, AZ, and Portland, OR. Int. J. Climatol. 32 (13), 2020–2032.
Middel, A., et al., 2014. Impact of urban form and design on mid-afternoon microclimate in Phoenix Local Climate Zones. Landsc. Urban Plan. 122, 16–28.
Mills, G., et al., 2010. Climate information for improved planning and management of mega cities (needs perspective). Procedia Environ. Sci. 1 (1), 228–246.
Myrup, L., 1969. A numerical model of the urban heat island. J. Appl. Meteorol. 8 (6), 908–918.
Offerle, B., Grimmond, C., Oke, T., 2003. Parameterization of net all-wave radiation for urban areas. J. Appl. Meteorol. 42 (8), 1157–1173.
Oke, T., 2006. Towards better scientific communication in urban climate. Theor. Appl. Climatol. (84), 179–190.
Onomura, S., et al., 2015. Meteorological forcing data for urban outdoor thermal comfort models from a coupled convective boundary layer and surface energy balance scheme. Urban Climate 11 (March 2015), 1–23.
Sailor, D., Vasireddy, C., 2006. Correcting aggregate energy consumption data to account for variability in local weather. Environ. Model. Softw. 21 (5), 733–738.
Schmid, H.P., Cleugh, H.A., Grimmond, C.S.B., Oke, T.R., 1991. Spatial variability of energy fluxes in suburban terrain. Bound.-Layer Meteorol. 54, 249–276. http://dx.doi.org/10.1007/BF00183956.
See, L., et al., 2015. Generating WUDAPT's Specific Scale-dependent Urban Modeling and Activity Parameters: Collection of Level 1 and Level 2 Data. Toulouse, France, 20–24th July 2015. pp. 1–4.
Shcherbakov, M., et al., 2013. A survey of forecast error measures. World Appl. Sci. J. 24, 171–176.
Shir, C., Shieh, J., 1974. A generalized urban air pollution model and its application to the study of SO2 distributions in the St. Louis Metropolitan Area. J. Appl. Meteorol. 13 (2), 185–204.
Stewart, I., Oke, T., 2012. Local climate zones for urban temperature studies. Bull. Am. Meteorol. Soc. 93, 1879–1900.
Stewart, I., Oke, T., Krayenhoff, E., 2014. Evaluation of the 'local climate zone' scheme using temperature observations and model simulations. Int. J. Climatol. 34 (4), 1062–1080.
Sunderland, K., Mills, G., Conlon, M., 2013. Estimating the wind resource in an urban area: a case study of micro-wind generation potential in Dublin, Ireland. J. Wind Eng. Ind. Aerodyn. 118 (July), 44–53.
Tanner, B.D., Swiatek, E., Greene, J.P., 1993. Density fluctuations and use of krypton hygrometer in surface flux measurements. Proceedings of the 1993 National Conference on Irrigation and Drainage Engineering (8), Park City, Utah, 21-23 July 1993. Irrigation and Drainage Division, American Society of Civil Engineers.
Taha, H., Akbari, H., Rosenfeld, A., Huang, J., 1988. Residential cooling loads and the urban heat island—the effects of albedo. Build. Environ. 23 (4), 271–283.
Taylor, K.E., 2001. Summarizing multiple aspects of model performance in a single diagram. J. Geophys. Res.: Atmos. 106, 7183–7192. http://dx.doi.org/10.1029/2000JD900719.
Vickers, D., Mahrt, L., 1997. Quality control and flux sampling problems for tower and aircraft data. J. Atmos. Ocean. Technol. 14, 512–526. http://dx.doi.org/10.1175/1520-0426(1997)014<0512:QCAFSP>2.0.CO;2.
Webb, E.K., Pearman, G.I., Leuning, R., 1980. Correction of flux measurements for density effects due to heat and water vapour transfer. Q. J. R. Meteorol. Soc. 106, 85–100. http://dx.doi.org/10.1002/qj.49710644707.
Wilczak, J.M., Oncley, S.P., Stage, S.A., 2001. Sonic Anemometer Tilt Correction Algorithms. Bound.-Layer Meteorol. 99, 127–150. http://dx.doi.org/10.1023/A:1018966204465.